T H E E F F E C T S

OF

SURFACE FRICTION IN A SYNOPTIC SCALE NUMERICAL MODEL

B Y

G Ü N T E R F I S C H E R

UNIVERSITÄT HAMBURG, METEOROLOGISCHES INSTITUT

1. Introduction

A series of numerical calculations with a baroclinic primitive equation model has been performed in order to investigate the influence of surface friction on the development of synoptic-scale disturbances.

In such a model there exist in principle two different ways to handle the turbulent momentum flux within the boundary layer:

(i) the boundary layer is adequately resolved by computational levels which allow for a direct application of friction laws and adopt the constant-flux-layer-hypothesis, for example, as a lower boundary condition for the surface stress. This principle is applied in the GFDL-model.

(ii) the first computational level above the ground is placed near the top of the PBL. This has the consequence that the frictional processes have to be linked in some reasonable way to known variables of the free atmosphere and known conditions at the surface.

The latter method, though less accurate, is the most common one since it saves computer time. We also shall adopt this principle for all our five numerical experiments (out of fifteen) to be presented here. The experiments differ however, in the way the frictional effects are simulated or parameterized in the numerical model. (For reference see: Fischer et al 1973,

2. The numerical Model

The computations are based upon a five-layer primitive equation model confined within a zonal channel. The vertical coordinate is $\sigma = p/p_s$ (though our results will be presented in the p-system) where p_s is surface pressure. The horizontal grid increments have been chosen to

$$\Delta x = \Delta y = 300 \text{ km}$$

The underlying equations are:

$$\frac{\partial u}{\partial t} = -\vec{V}\cdot\nabla u - \dot{\sigma}\frac{\partial u}{\partial \sigma} + fv - \frac{\partial \phi}{\partial x} - \frac{RT}{p^*}\frac{\partial p^*}{\partial x} + K_h\nabla^2 u - \frac{g}{p_s}\frac{\partial \tau_x}{\partial \sigma} \tag{2.1}$$

$$\frac{\partial \bar{v}}{\partial t} = -\vec{V}\cdot\nabla v - \dot{\sigma}\frac{\partial v}{\partial \sigma} - fu - \frac{\partial \phi}{\partial y} - \frac{RT}{p^*}\frac{\partial p^*}{\partial y} + K_h\nabla^2 v - \frac{g}{p_s}\frac{\partial \tau_y}{\partial \sigma} \tag{2.2}$$

$$\frac{\partial \Theta}{\partial t} = -\vec{V}\cdot\nabla\Theta - \dot{\sigma}\frac{\partial \Theta}{\partial \sigma} + K_h\nabla^2\Theta \tag{2.3}$$

$$\frac{\partial p^*}{\partial t} = -\int_0^1 \nabla\cdot(p^*\vec{V})\, d\sigma \tag{2.4}$$

$$\frac{\partial \dot{\sigma}}{\partial \sigma} = -\frac{1}{p^*}\left\{\nabla\cdot(p^*\vec{V}) - \int_0^1 \nabla\cdot(p^*\vec{V})\, d\sigma\right\} \tag{2.5}$$

$$\frac{\partial \phi}{\partial \sigma} = -\frac{RT}{\sigma} \tag{2.6}$$

where $p^* = p_s/p_o$ and p_o = 1000 mb. The other variables have their usual meaning.

The system has been integrated numerically with a time staggered Lax-Wendroff scheme.

3. Initial Conditions

The wind and mass fields are initially in geostrophic balance. The former consists of barotropic disturbances represented by the geostrophic stream function $\psi'(x,y)$ which is superimposed on a baroclinic zonal current $\bar{u}(x,p)$

$$\bar{u} = 2(1-p/p_o)\, U_1 \left\{ \left(1 - \cos \frac{2\pi}{B} y \right) + q \left(1 - \cos \frac{4\pi}{B} y \right) \right\} \qquad (3.1)$$

$$\psi' = \sum_{n=1}^{5} (-1)^n \frac{v_m L}{4\pi n} \left(1 - \cos \frac{2\pi}{B} y\right) \sin \frac{2\pi n}{L} x \qquad (3.2)$$

The parameters attain the following values :

U_1 = 9 m/s

v_m = 3 m/s

q = 0.5

f = $10^{-4} s^{-1}$ = constant

L = 12000 km (length of the channel)

B = 6000 km (width of the channel)

Furthermore we chose

K_h = 10^5 m^2/s

s^2 = 0.5

whereby s^2 is a measure of the static stability initially prescribed in the model.

$$s^2 = -p_o^2 \pi^2 / f^2 B^2 \frac{1}{\rho\theta} \frac{\partial\theta}{\partial p}$$

The surface pressure field and the 500mb height field at t = 0 are shown in fig. 1.

4. Boundary Layer Parameterizations

Our model does not contain moist convection and condensation processes. Nor is turbulent heat transfer in the vertical implied. Thus the only turbulent transport in the boundary layer is that of momentum. The latter has to be related to conditions at the surface and in the first computational level from below which is located at $\sigma = \sigma_H = 0.9$ ($p \gtrsim 900$ mb). We assume that this level coincides with the top of the planetary boundary layer (Height $H \approx 1000$ mb); we therefore prescribe that the stress vector $\vec{\tau}$ (the momentum flux) has some finite value for $\sigma > \sigma_H$ and vanishes for $\sigma \leq \sigma_H$. With these assumptions in mind we will discuss in the next section how the frictional force $-\frac{g}{p_s} \frac{\partial \vec{\tau}}{\partial \sigma}$ (see (2.1) and (2.2)) has been incorporated in the finite difference scheme.

5. Finite Difference Representation of Surface Friction Approach I

Adopting the vertical grid system of fig. 2 the frictional force at the computational level $\sigma_H = 0.9$ can be replaced very simply by its finite difference analogue

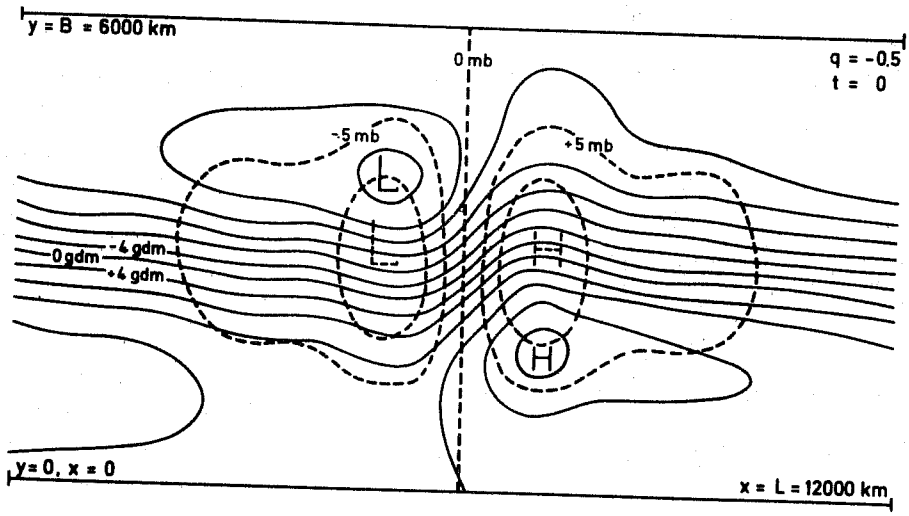

Fig. 1: Initial fields of surface pressure (dashed lines) and 500 mb height (solid lines)

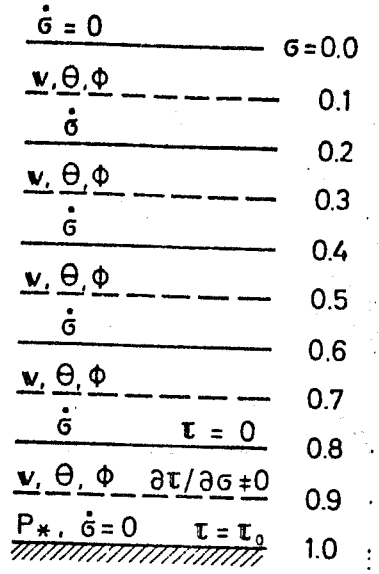

Fig. 2: Vertical grid resolution for Approach I.

$$-\frac{g}{p_s}\frac{\partial \tau}{\partial \sigma} - \frac{g\tau}{0.2p_s} \qquad (5.1)$$

Thus the frictional processes in the boundary layer are expressible through the surface stress τ_o. The problem is reduced to find a proper way to relate the surface stress to other variables. Most commonly this is done by setting

$$\tau_o = \rho C_D |v_o| v_o \qquad (5.2)$$

The question arises then how unknown surface wind v_o is evaluated. This problem will be discussed later in 6.

Approach II

In this case the numerical model is restricted to the free atmosphere in that it does not employ the condition of vanishing vertical velocity at the ground but rather uses a frictionally induced vertical velocity $\dot{\sigma}_H$ as a lower boundary condition at $\sigma = \sigma_H$. This is made possible by applying the simplified steady state vorticity equation which relates the vertical velocity at the top of the boundary layer to curl τ_o

In order to realise this idea in a favourable manner the vertical grid system of fig. 3 has been adopted. Starting from the simplified vorticity equation(which is derived under the assumption of a balance between Coriolis-pressure and friction forces).

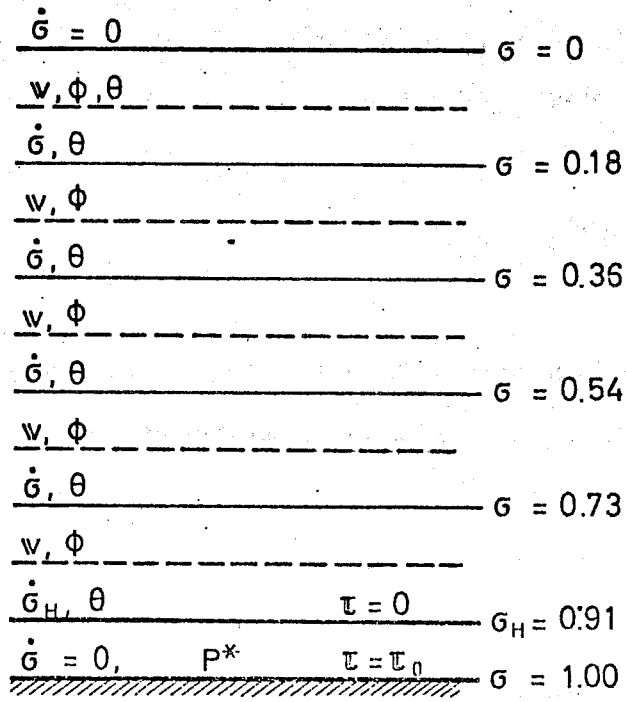

fig.3 Vertical grid resolution for Approach II

$$f\nabla\cdot(p^{*}\vec{v}) = -\frac{g}{p_o}\frac{\partial}{\partial\sigma}\,\mathrm{curl}\,\vec{\tau} - J(p^{*},\phi-RT) \qquad (5.3)$$

one obtains with the aid of the continuity equation in the form

$$\frac{\partial(p^{*}\dot{\sigma})}{\partial\sigma} = -\frac{\partial p^{*}}{\partial t} - \nabla\cdot(p^{*}\vec{v}) \qquad (5.4)$$

the following expression for the vertical velocity :

$$\dot{\sigma}_H = \frac{1-\sigma_H}{p^{*}}\left\{\int_0^{\sigma_H}\nabla\cdot(p^{*}\vec{v})\,d\sigma + \frac{\sigma_H}{f}\,J(p^{*},\phi-RT)\right\} - \frac{g\sigma_H}{fp_s}\,\mathrm{curl}\,\vec{\tau}_o \qquad (5.5)$$

The pressure tendency at the surface is given by:

$$\frac{\partial p^{*}}{\partial t} = -\frac{1}{\sigma_H}\int_0^{\sigma_H}\nabla\cdot(p^{*}\vec{v})\,d\sigma - \frac{p^{*}}{\sigma_H}\dot{\sigma}_H \qquad (5.6)$$

As can be seen only variables of the free atmosphere enter into (5.5) and (5.6) together with the surface stress which can be handled according to (5.2).

6. The Evaluation of $\vec{\tau}_o$

In order to get the surface stress we adopted either (5.2) or the so-called resistance law. The first case requires that the surface wind has to be specified. To achieve this, two methods, denoted Method a and Method c have been employed. The resistance law will be called Method b . In all instances a barotropic boundary layer is assumed.

Method a uses the Taylor spiral, yielding a connection between the surface wind and the geostrophic wind $\vec{v}_{go}$ in the followin form:

$$\vec{v}_o = \ell \tilde{M} \vec{v}_{go} \tag{6.1}$$

where

$$\ell = \cos\alpha_o - \sin\alpha_o ; \quad \tilde{M} = \begin{pmatrix} \cos\alpha_o & -\sin\alpha_o \\ \sin\alpha_o & \cos\alpha_o \end{pmatrix} \tag{6.2}$$

To obtain the cross-isobar angle α_o we recall that the Taylor solution has the boundary condition

$$A \frac{\partial \vec{v}}{\partial z} = \rho r \vec{v}_o \tag{6.3}$$

where A is the exchange coefficient assumed to be constant. Though r should be a constant this quantit y was identified according to (5.2) with

$$r = C_D |\vec{v}_o| \tag{6.4}$$

If this is done α_o can be derived from

$$\frac{\sin\alpha_o}{\ell} = \rho C_D |\vec{v}_{go}| (2Af\rho)^{-1/2} \approx \frac{\rho C_D |\vec{v}_{go}| H}{2\pi A} \tag{6.5}$$

α_o increases with increasing v_{go}

Thus the surface stress is given by:

$$\vec{\tau}_o = \rho C_D |\vec{v}_{go}| \ell^2 \tilde{M} \vec{v}_{go} \tag{6.6}$$

Method b applies the resistance law in the form

$$\left(\ell u \frac{u_*}{f z_o} - M \right)^2 = \left(\frac{k|v_{go}|}{U_*} \right)^2 - N^2 ;$$

$$\sin \alpha_o = \frac{N U_*}{k|v|_{go}} ; \quad U_*^2 = \frac{\tau_o}{\rho} \qquad (6.7)$$

where according to Wippermann (1970) M=0.9 and N=4.5 have been chosen. α_o decreases slightly with increasing v_{go}

Method c is used in the NCAR-model (Kasahara 1967). From the relationship according to (5.2)

$$A \left(\frac{\partial v}{\partial z} \right)_o = \rho C_D |v_o| v_o \qquad (6.8)$$

the finite difference formulation

$$\frac{A}{H} \left(v_H - v_o \right) = \rho C_D |v_o| v_o$$

can be derived relating v_o to the computed wind v_H at $\sigma = \sigma_H$ when the vertical grid system of fig. 2 is employed. The surface stress follows from (5.2).

Approaches I and II have been combined with methods a,b and c yielding the parameterizations :Ia, Ib, Ic, IIa. These numbers will serve to define the kind of experiment. Moreover, there is an experiment 0 without any boundary layer representation. The "frictional" parameters representing land

conditions assume the following values :

$$A = 40 gm/cm\ s \qquad C_D = 0.012 \qquad z_o = 26\ cm. \tag{6.10}$$

The values have been chosen in such a way that from the physical point of view there should be no difference. It should be mentioned that an experiment performed with a stability-dependent A yielded practically the same results.

7. Pressure Field Forecasts

All experiments were run for 150 hours. In this period the original low and high pressure centres at the surface (see fig.1) denoted by L_1 and H_1 respectively show quite a substantial intensification in most cases as can be detected from fig. 4. At about t = 80 h a secondary cyclone (L_2) appears at the surface in front of an upper air trough together with a ridge (H_2) . This "young" wave disturbance is located after 150 hours at the "western" half of the channel and has a pressure deviation of about -20 mb. At the same time L_1 has assumed the structure of an almost occluded cyclone.

To demonstrate the effect of our friction formulations, we will look in table 2 upon the depths of L_1, L_2, H_1 and H_2 (deviation from 1000 mb) at t = 100 h (first number) and t = 150 h (second number)

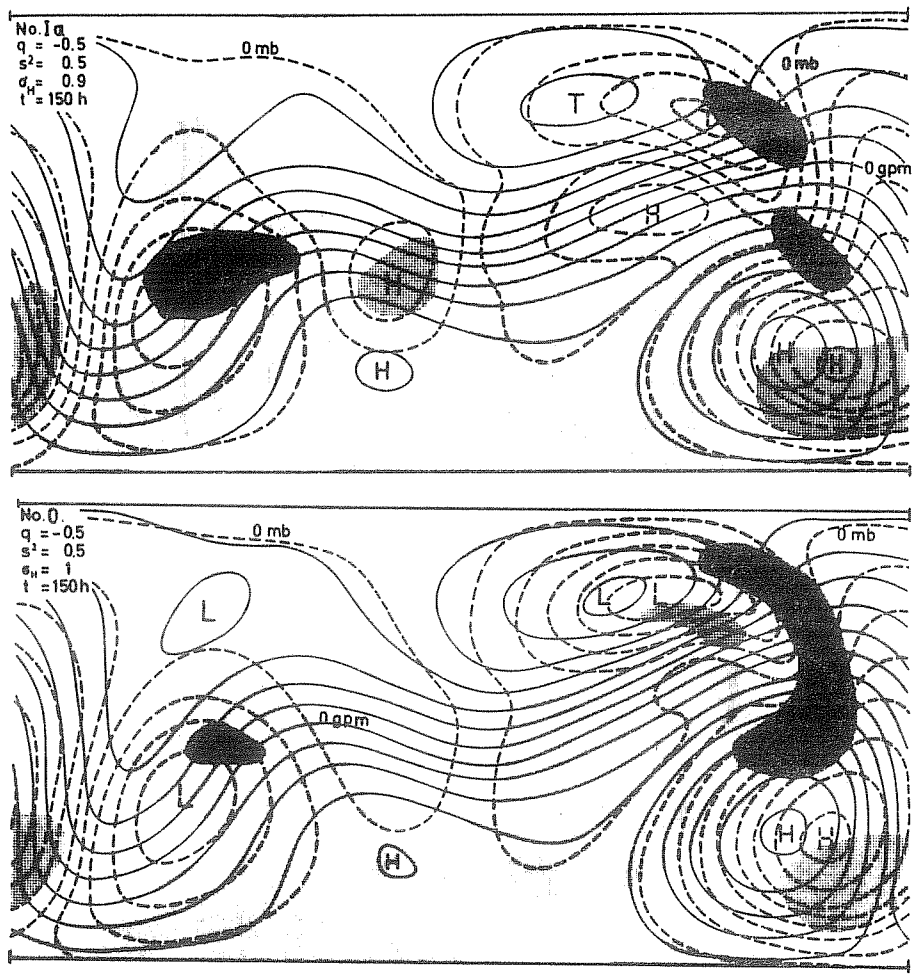

Fig. 4: Synoptic maps at t=150 hours. Surface isobars and 500 mb contours as in Fig. 1.
Shaded areas mark the intensity of vertical motions in 800 mb ($|\omega| > 1$ mb/h)
(a) : experiment 0
(b) : experiment Ia

With respect to L_1 this cyclone shows a tendency to weaken after 100 hours in nearly all cases. This process becomes quite pronounced when surface friction is present with the exception of Ic where the pressure continues to fall slightly. On the other hand there appears in all experiments an amplification of L_2 ,which seems nearly not affected by surface friction. The formulations Ia and Ib yield even a deeper pressure of L_2 than the frictionless case O. The original high H_1 intensifies from t = 100 h to t = 150 h in each experiment and seems thus less influenced by surface friction than L_1 .

In general there is only a small difference between Ia and Ib. It is interesting to note that these cases yield a strong damping of X the occluded system L_1 and a slight intensification of the "young" wave L_2 compared with experiment O. The friction-formulation IIa exerts a relatively strong damping on all pressure patterns, especially on L_1 and H_1. Experiment Ic shows a weaker L_2 and a stronger L_1 than Ia and Ib and is thus qualitatively closer to the frictionless case O.

EXPERIMENT	L_1	L_2	H_1		H_2	
O	-29.0-28.9	-8.1-19.3	26.6	36.1	---	3.8
Ia	-25.6-21.0	-9.2-20.4	25.3	35.5	1.6	8.5
Ib	-22.4-19.0	-9.6-20.9	25.3	34.6	2.3	8.7
Ic	-23.8-24.3	-7.9-18.2	23.8	31.2	---	3.8
IIa	-14.5-11.9	-7.6-16.1	20.6	23.8	--	4.7

Tab.1

8. The Formation of Fronts

The temperature field at 900 mb responded quite sensibly when surface friction was introduced. Except in Exp.IIa it reacted in such a way that sharp temperature contrasts were generated, which were much more pronounced than in the "frictionless" Exp.O. This fact can be seen in fig. 5 and in the following table (Tab.2). The latter demonstrates how the temperature gradients increase with time in the vicinity of L_1, where a warm ("W) front and a cold ("C") front evolves.

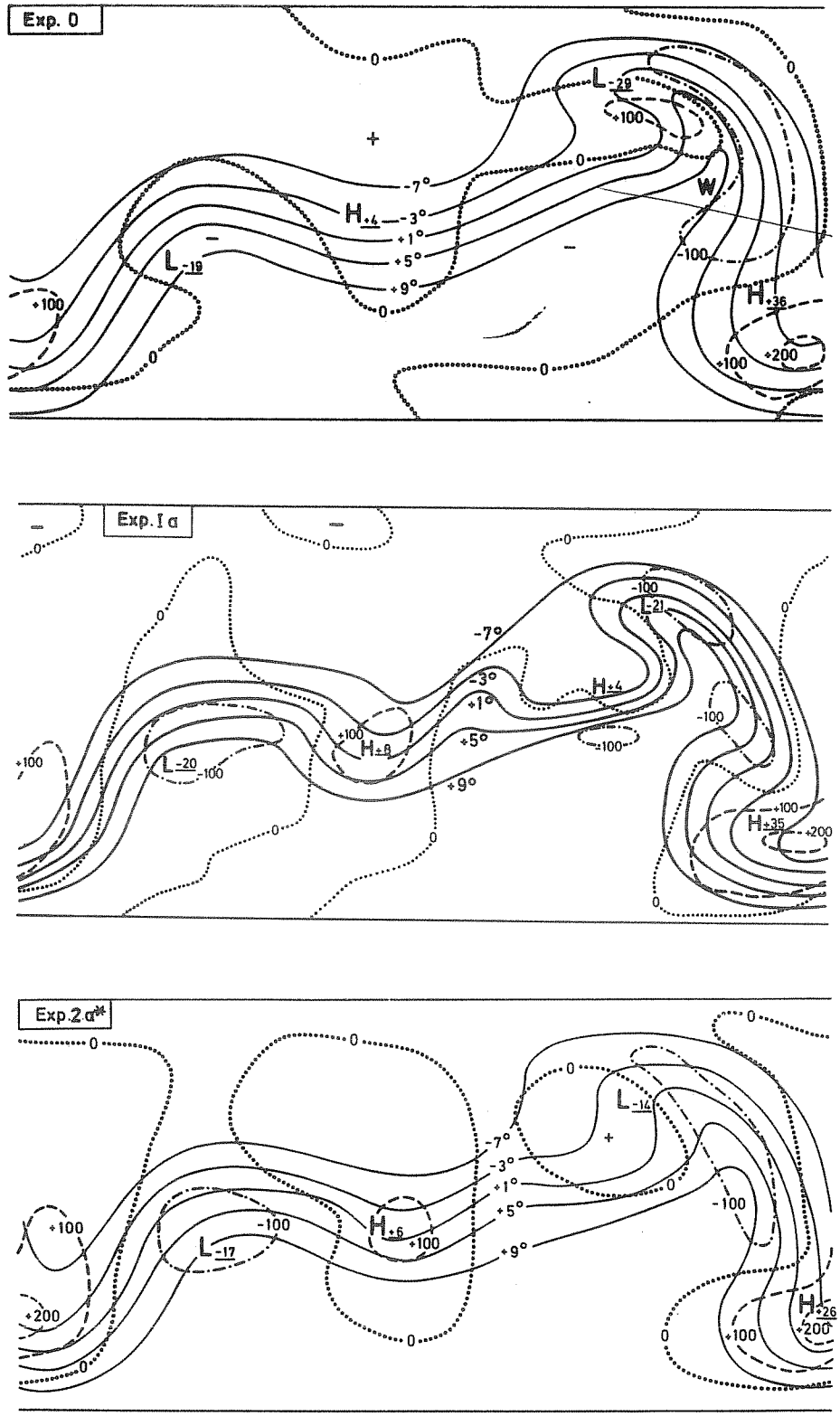

Fig.5 Temperature fields (solid lines) in 900 mb and field of vertical motion (dashed lines, dotted lines and dash-dotted lines) in 800 mb at t = 100 h . The letters H and L mark the positions of the Highs and Lows, respectively, in the surface pressure field. The underlined numbers denote the pressure deviations from 1000 mb in the centres of H and L. Temperature in °C pressure, deviations in mb, vertical motions in mb/100 hours

(a): Experiment O,(b): experiment Ia,(c): experiment 2a* (slightly different version of 2a)

t(h)	Exp.O	Exp.Ia	Exp.Ic	Exp.IIa	
0	13.0	13.0	13.0	13.0	$\lvert\nabla T\rvert$
50	16.4 W	27.2 W	15.0 W	18.5 W	$^{o}C/1000$ km
		24.9 C	13.1 C	14.1 C	
100	19.0 W	28.1 W	17.1 W	17.2 W	
	15.1 C	32.3 C	14.1 C	13.4 C	
150	18.8 W	25.9 W	17.8 W	17.7 W	
	16 3 C	32.2 C	14.6 C	11.7 C	Table 2

From the distribution of surface pressure, 900 mb temperature and 800 mb vertical p-velocity, it is possible to fix quite accurately the warm front, the cold front and the occlusion connected with L_1 (see fig.6).

To get more insight into this interesting feature for cases O and Ia cross-sections have been drawn perpendicular to the cold front and the warm front "south" of L_1 . From fig. 7 it can be seen that the temperature structure of Exp. O was not altered qualitatively very much after 100 hours whereas Exp. Ia exhibits a pronounced change in tis vertical distribution in that a strong inversion in the lower layers is observed. Thus the formation of sharp fronts in Exp.Ia is confined to a relatively shallow layer (fig.7b).

The result that surface friction contributes to a sharpening of temperature contrasts was also obtained by Williams (1974) though in his model it appeared less accentuated. On the other hand Hoskins and Bretherton (1972) state that surface friction is frontolytic. The latter authors give an explanation for the formation of fronts on the basis of the conservation of potential vorticity. Their explanation is mathematically founded on the basis that potential vorticity is a positive quantity.

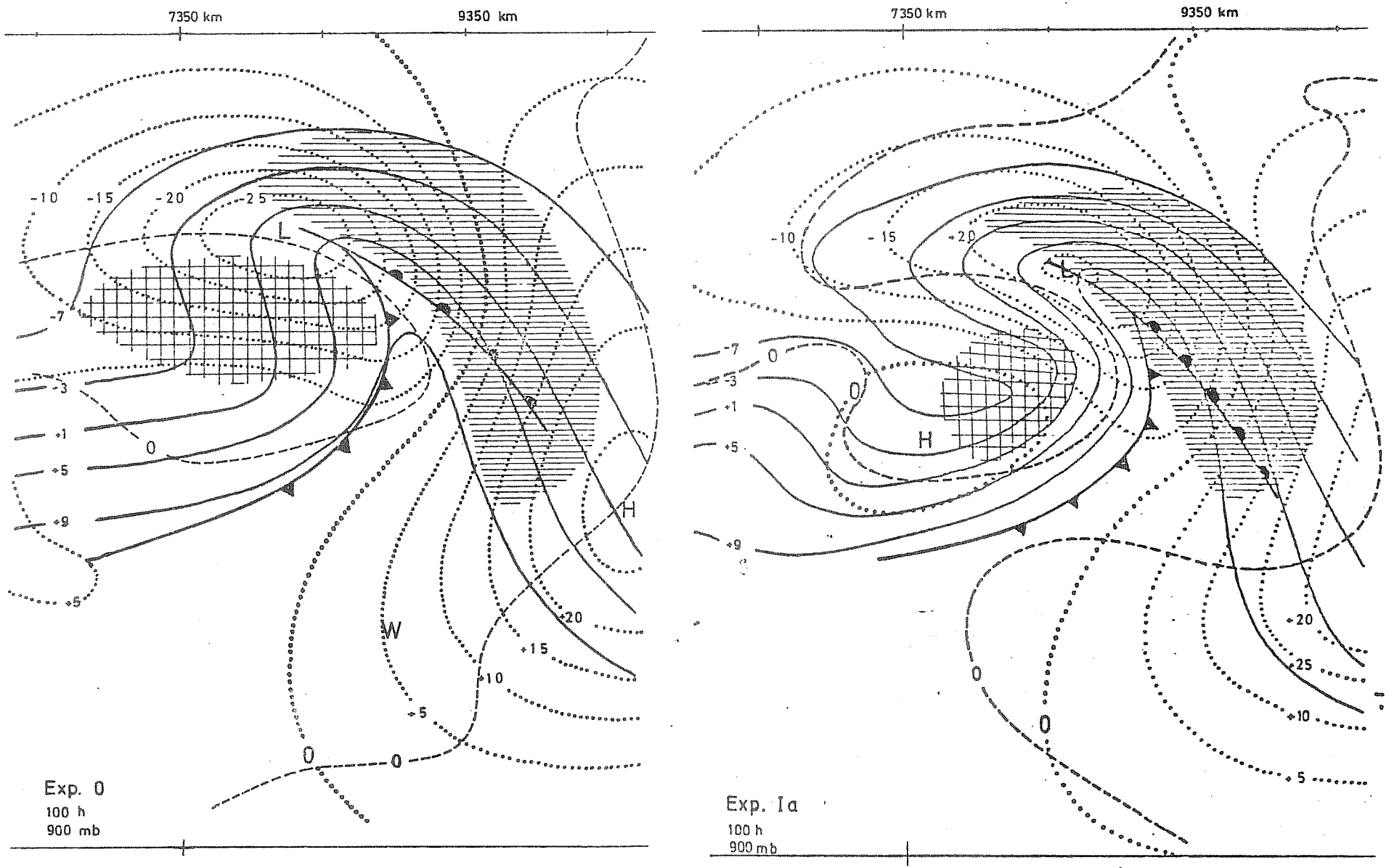

Fig.6 Frontal structure in the vicinity of L_1 at t = 100 h.
Surface isobars (dotted lines), 900 mb isotherms (solid lines).
Hatched areas denote $/\omega/ \geq 1 \frac{mb}{n}$, dashed lines ω=0 in 800 mb

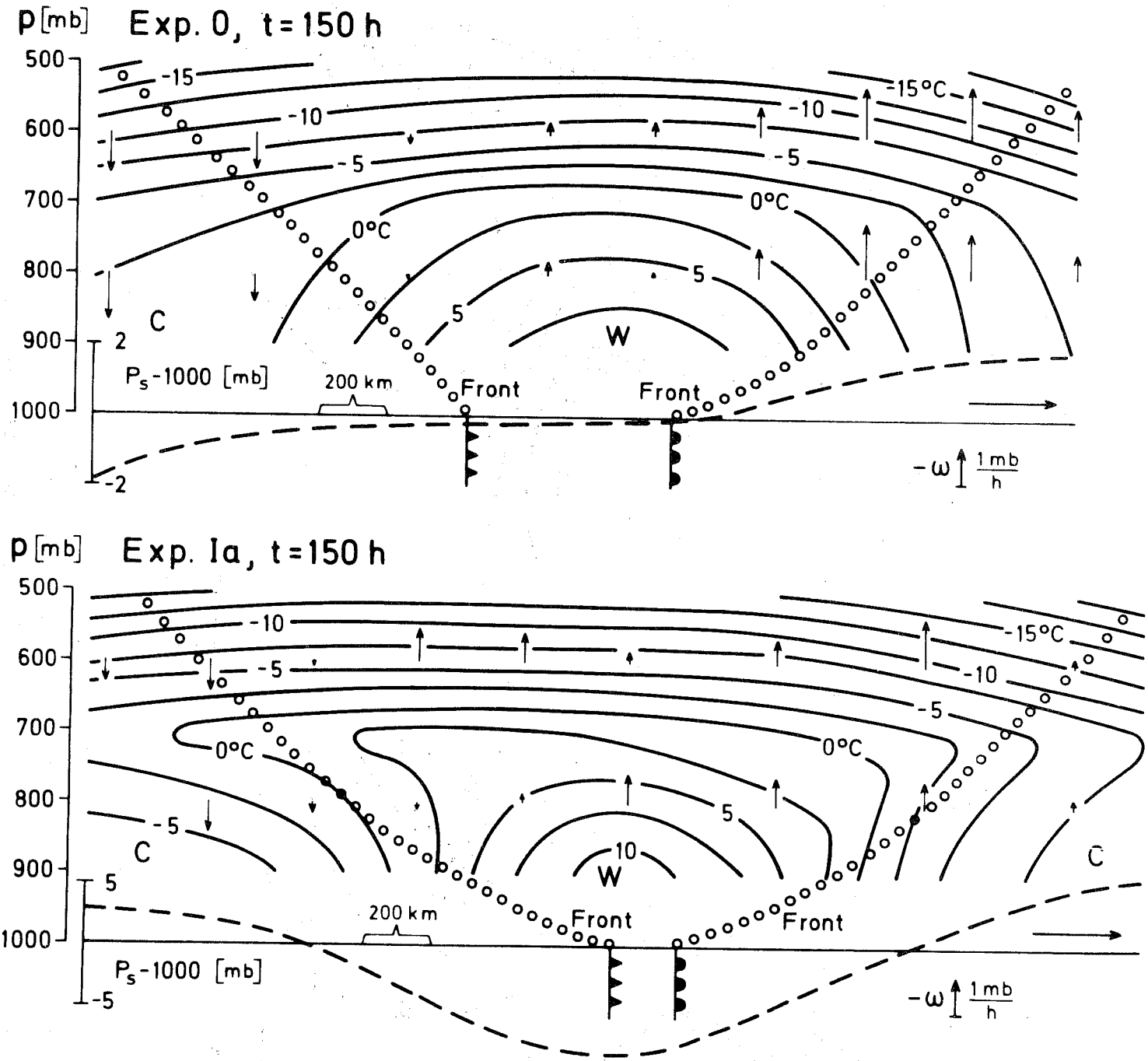

Fig. 7: Vertical cross-section of temperature and vertical velocity through the warm tongue associated with L_1.

9. Frontogenetic Functions

We shall attempt to get further insight into the problem of front formation by considering some relevant relationships evolving from the basic equations.

Thus, from (2.3) one obtains after certain manipulations

$$\underset{(F)}{\frac{T}{\Theta}\frac{d}{dt}\left|\Theta\right|} = -\frac{1}{\Delta T}\left\{\frac{\partial u}{\partial x}\left(\frac{\partial T}{\partial x}\right)^2 + \frac{\partial v}{\partial y}\left(\frac{\partial T}{\partial y}\right)^2 + \underset{(A)}{\left(\frac{\partial v}{\partial x}+\frac{\partial u}{\partial y}\right)\frac{\partial T}{\partial x}\frac{\partial T}{\partial y}}\right\} + S^2\underset{(B)}{\left\{\frac{\partial \omega}{\partial x}\frac{\partial T}{\partial x} + \frac{\partial \omega}{\partial y}\frac{\partial T}{\partial y}\right\}} \qquad (9.1)$$

where $S^2 = -\frac{T}{\Theta}\frac{\partial \Theta}{\partial p}$

which relates the individual change of the temperature gradient (F) to kinematic properties (horizontal divergence and deformation) in term (A) and vertical circulations implied in term (B).
As in frontal systems there exists in general a thermally direct circulation, (B) should be negative. Then (A) must be positive to generate fronts.

Another suitable expression follows from (2.1) and (2.2) together with (2.3) and (2.6) (if transformed to the p-system)

$$\frac{d}{dt}\left\{\frac{\partial u}{\partial p}\frac{\partial \Theta}{\partial y} - \frac{\partial v}{\partial p}\frac{\partial \Theta}{\partial x}\right\} = \left(\xi + f\right)\left\{\frac{\partial \Theta}{\partial x}\frac{\partial u}{\partial p} + \frac{\partial \Theta}{\partial y}\frac{\partial v}{\partial p}\right\} + \frac{\partial \Theta}{\partial p}\left\{\frac{\partial \omega}{\partial x}\frac{\partial v}{\partial p} - \frac{\partial \omega}{\partial y}\frac{\partial u}{\partial p}\right\} - g\left\{\frac{\partial^2 \tau_x}{\partial p^2}\frac{\partial \Theta}{\partial y} - \frac{\partial^2 \tau_y}{\partial p^2}\frac{\partial \Theta}{\partial x}\right\} \qquad (9.2)$$

The left hand side term of (9.2) is proportional to the change of $(\nabla\theta)^2$ which can be seen if $\partial u/\partial p$ and $\partial v/\partial p$ are approximated geostrophically. It thus can be used to define another frontogenetic function (F^*). Because of

$$\frac{d}{dt}\left\{\frac{\partial\theta}{\partial p}(\xi+f)+\left(\frac{\partial u}{\partial p}\frac{\partial\theta}{\partial y}-\frac{\partial v}{\partial p}\frac{\partial\theta}{\partial x}\right)\right\}=g\left\{\frac{\partial^2\tau_x}{\partial p^2}\frac{\partial\theta}{\partial y}-\frac{\partial^2\tau_y}{\partial p^2}\frac{\partial\theta}{\partial x}\right\}- -g\frac{\partial\theta}{\partial p}\ \mathrm{curl}\ \frac{\partial\tau}{\partial p} \tag{9.3}$$

this function (F^*) is related to the change of the vertical component of potential vorticity, i.e. $d/dt\{(\zeta+f)\,\partial\theta/\partial p\}$ From (9.2) we get

$$\underset{(F^*)}{\frac{T}{\theta}\frac{d}{dt}\left|\nabla\theta_g\right|}=\frac{1-}{2p}\omega\left|\nabla T\right|+\underset{(A^*)}{\frac{fp(\xi+f)}{2R\left|\nabla T\right|}\left\{\frac{\partial T}{\partial x}\frac{\partial u}{\partial p}+\frac{\partial T}{\partial y}\frac{\partial v}{\partial p}\right\}}+$$

$$+\underset{(B^*)}{\frac{fpS^2}{2R\left|\nabla T\right|}\left\{\frac{\partial\omega}{\partial x}\frac{\partial v}{\partial p}-\frac{\partial\omega}{\partial y}\frac{\partial u}{\partial p}\right\}}-\underset{(C^*)}{\frac{gfp}{2R\left|\nabla T\right|}\left\{\frac{\partial^2\tau_x}{\partial p^2}\frac{\partial T}{\partial y}-\frac{\partial^2\tau_y}{\partial p^2}\frac{\partial T}{\partial x}\right\}} \tag{9.4}$$

(F^*) has the same dimension as (F), both quantities should be about equal. The subscript "g" denotes that the geostrophic approximation has been introduced.

The first term on the right hand side is relatively small and shall not be considered anymore. Term (B^*) is frontolytic for the same reason as term (B) in (9.1). Thus, for front generation, (A^*) + (C^*) has to be positive. Note that (A^*) vanishes, for geostrophic conditions. On the other hand (A^*) must have a positive contribution when the static stability increases and the motion is convergent as is generally

relationship

$$-\frac{T}{\Theta}\ \frac{d}{dt}\left(\frac{\partial\Theta}{\partial p}\right)=\left\{\frac{\partial u}{\partial p}\ \frac{\partial T}{\partial x}\ +\ \frac{\partial v}{\partial y}\ \frac{\partial T}{\partial y}\right\}+S^2\nabla\cdot\vec{v} \qquad (9.5)$$

which is also involved in (9.3) . Thus with no friction ($(C^*)=0$) there is a connection between front formation, increasing static stability and vorticity generation (provided $\nabla\cdot\vec{v}<0$). Looking on the distribution of horizontal divergence at 900 mb (Fig. 8) negative values occur at the warm front, whereas positive values are found behind the cold front, where the strongest temperature contrasts exist at 900 mb.
In the latter case so the positive divergence gives a positive contribution to the rate of change of static stability according to (9.5).

The following table (Table 3) displays the extreme values of terms (A), (B) in (9.1) and (A^*), (B^*) in (9.4) of the warm front (W) and cold front (C) for our experiments 0 and Ia.

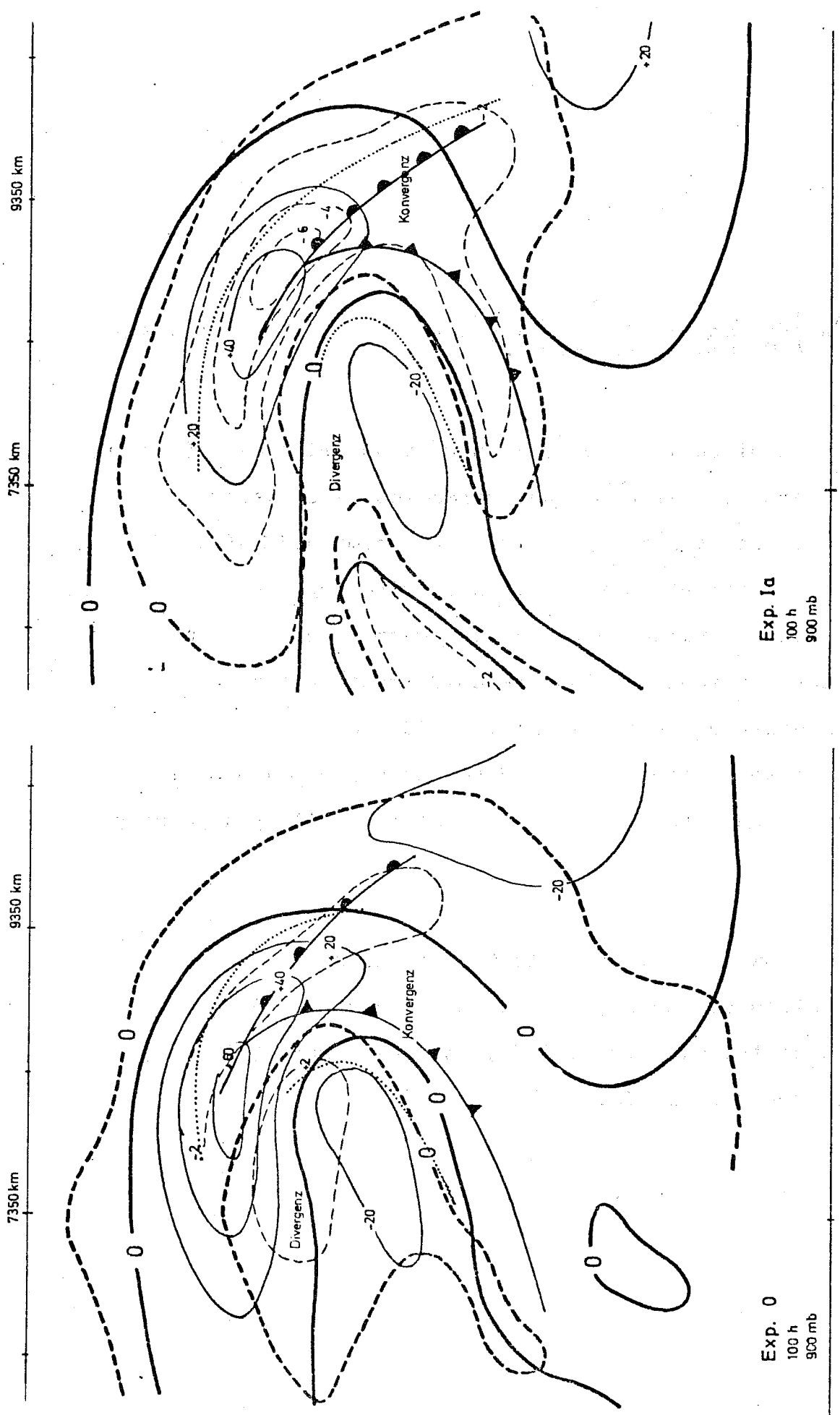

Fig.8 Fields of vorticity (solid lines) and horizontal divergence (dashed lines) in 900 mb (Units $10^{-6}s^{-1}$). Dotted lines denote zones of strongest temperature contrasts. Experiments 0 and Ia

		(A)	(B)	(F)= (A)+(B)	A^*	B^*	$(F^*)-(C^*)$ = $(A^*)+(B^*)$
Exp. Ia	t = 100	10.5 W	- 6.6 W	7.3 W	26.6 W	-2.9 W	26.9 W
		12.1 C	-10.9 C	7.1 C	13.8 C	-4.3 C	9.8 C
	t = 150	11.0 W	- 6.4 W	5.1 C	25.2 W	-3.7 W	23.3 W
		9.7 C	-10.3 C	6.4 C	11.1 C	-3.4 C	8.9 C
Exp. O	t = 100	14.0 W	- 7.6 W	16.8 W	12.1 W	-3.9 W	16.8 W
		8.8 C	- 7.7 C	5.4 C	6.5 C	-4.2 C	4.3 C
	t = 150	10.6 W	- 6.1 W	13.5 W	9.2 W	-3.3 W	11.4 W
		8.2 C	- 5.5 C	2.9 C	4.4 C	-2.6 C	3.7 C

Table 3 Units $\left[10^{-8}\ {}^{o}K\ .\ km^{-1}\ s^{-1}\right]$

In the "frictionless" Exp.0 ($(C^*) = 0$) there is quite good agreement between F and F^* . This can be expected to hold also for Exp. Ia. It follows then that (C^*) is negative. This result does not imply, however, that surface friction is frontolytic since frictional effects also enter into (A^*). There they cause quite a substantial positive contribution that apparently overbalances (C^*).

Our former results that surface friction yields stronger temperature gradients are only partly reflected by the values of (F). Unfortunately (C^*) could not be evaluated accurately enough.

A synoptic view of A,B and A^*, B^* is given in fig. 9 and fig.10 respectively.

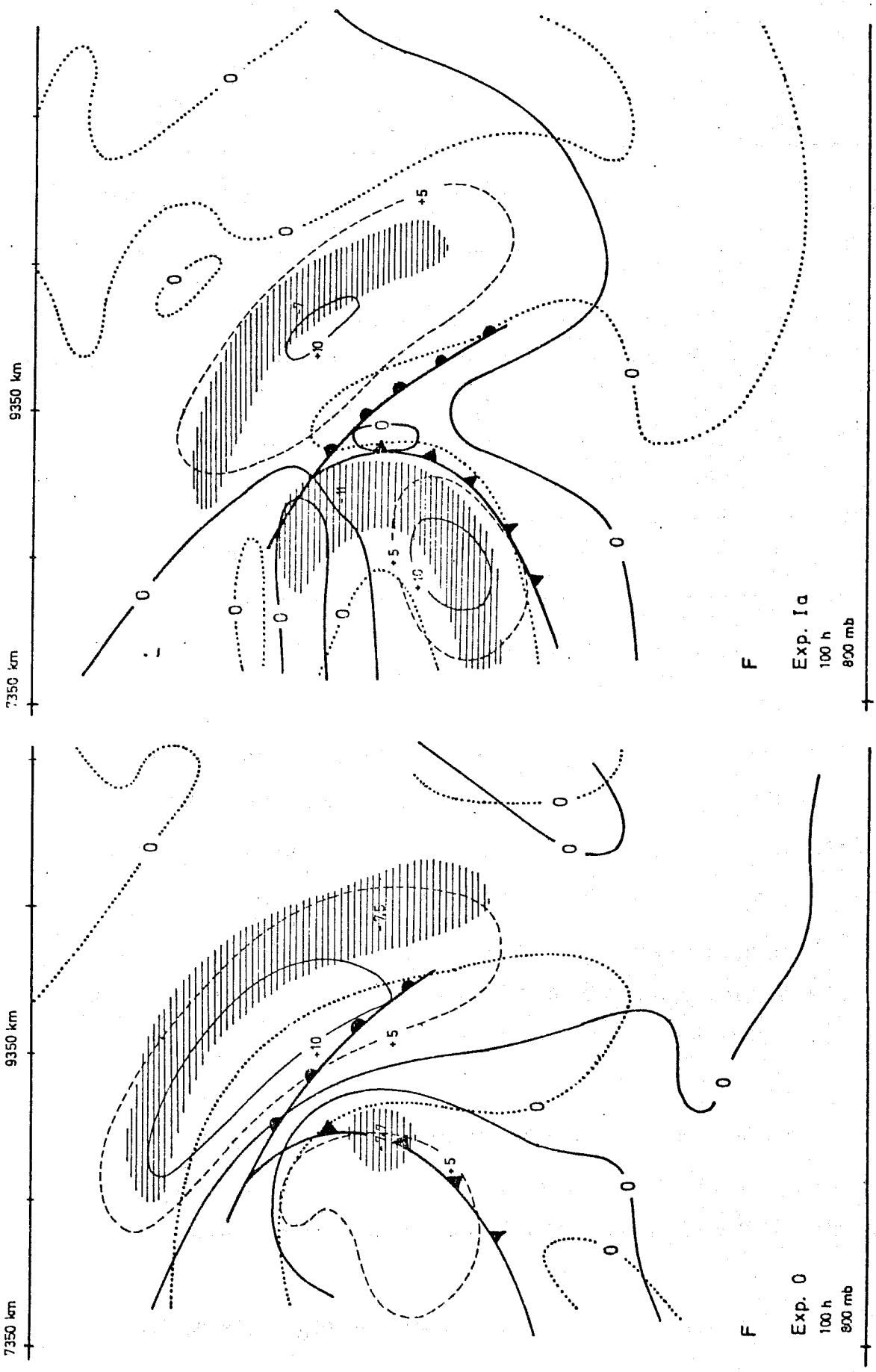

Fig. 9 The quantities A (solid and dashed lines) and B of (9.1) in Units 10^{-8} °C $km^{-1}s^{-1}$. Dotted lines: B=0. Shaded areas B<-5. Experiments 0 and Ia

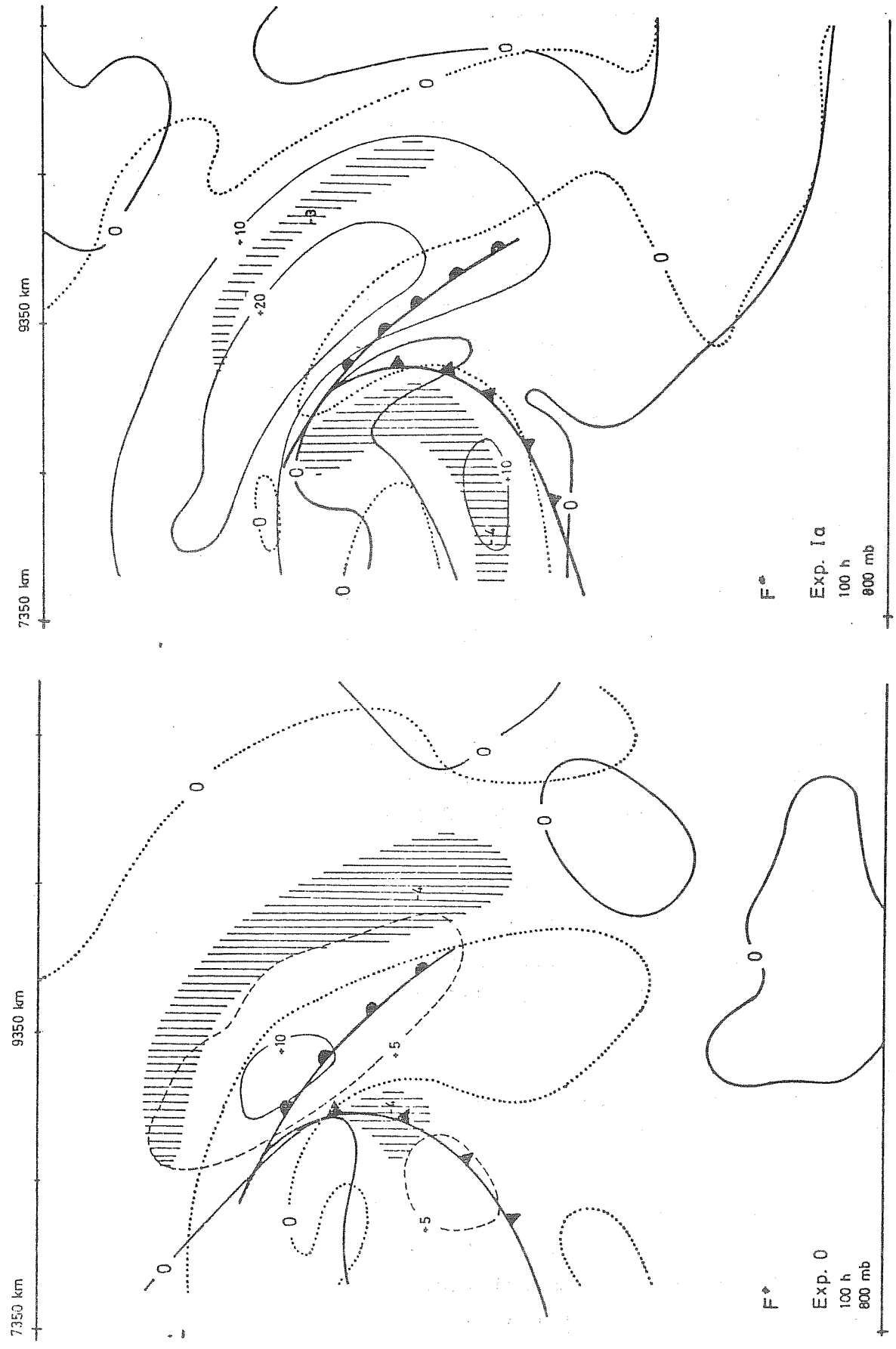

Fig.10 The quantities A^{*} (solid and dashed lines) and B^{*} of (9.4) in Units 10^{-8} °C $km^{-1}s^{-1}$. Dotted lines: $B^{*}=0$, shaded areas $B^{*} \leq -2.5$. Experiments 0 and Ia.

A. REFERENCES ON SURFACE FRICTION

Boye,H.,1974:
Numerische Rechnungen unter Beruecksichtigung der Ekman Schicht in einem baroklinen Vorhersagemodell. Hamb. Geophysik.Einzelschriften 20,1974, 103 pages.

Charnock,H. and T.H. Ellison,1967:
The boundary layer in relation to large-scale motions of the atmosphere and ocean. Report of the Study Conference on Global atmospheric Research Programme (GARP) Stockholm, June 28-July 11, 1967. Appendix III,1-16.

Clarke, R.H.,1970:
Recommended methods for the treatment of the boundary layer in numerical models.
Australian Meteorological Magazine 18, 51-71.

Deardorff,J.W.,1972:
Parameterization of the planetary boundary layer for use in general circulation models.
Monthly Weather Review, 100,93-106.

Delsol,F., K. Miyakoda and R.H. Clarke, 1971:
Parameterized processes in the surface boundary layer of an atmospheric circulation model.
Quart. J. Roy.Met.Soc. 97, 181-208.

Eady, E.T.,1949:
Long waves and cyclone waves.
Tellus 1/3, 33-52.

Everson, P.J. and D.R. Davies,1972:
Ekman boundary layer interactions in a numerical model of the general circulation.
Quart.J.Roy.Met.Soc.98,412-419

Fischer, G., E. Heise, V. Renner, 1973:
Studies on barotropic and baroclinic energy conversion in wave number regime .
Beitr. Phys.Atm. 46, 1-21.

Fischer, G., E. Heise, V. Renner, 1973:
The effect of surface friction on the development of cyclone waves in a numerical model.
Beitr. Phys.Atm. 46, 157-181.

Fortak, H., 1969:
Die Parameterisierung der Divergenz des vertikal gemittelten Impulsstromtensors der planetarischen Grenzschicht.
Veroeff. Inst . f. Theoretische Meteorologie der Freien Universitaet Berlin .

Graystone, P., 1962:
The introduction of topographic and frictional effects in a baroclinic model.
Quart.J.Roy.Met.Soc. 88, 256-270

Haltiner, G.J. and D.E. Caverly, 1965:
The influence of friction on the growth and structure of baroclinic waves.
Quart.J.Roy.Met.Soc. 91, 209-214

Hasse, L., 1968:
Zur Bestimmung der vertikalen Transporte von Impuls und fuehlbarer Waerme in der wassernahen Luftschicht ueber See.
Hamburger Geophysik.Einzelschriften 11.

Holloway Jr., J.L. and S. Manabe, 1971:
Simulation of climate by a global general circulation model. I Hydrologic cycle and heat balance.
Monthly Weather Review 99, 335-370

Holopainen,E.O.,1961:
On the effect of friction on baroclinic waves.
Tellus 13, 363-367.

Kung,E.C.,1966:
Kinetic energy generation and dissipation in the large-scale atmospheric circulation.
Monthly Weather Review 94,67-82.

Petterssen,S.,1956:
Weather analysis and forecasting.
Volume I: Motion and motion systems.
Mc Graw-Hill Book Company, Inc., New York, Toronto, London, 428 pages.

Phillips,N.A.,1963:
Geostrophic motion.
Rev. Geophys. 1, 123-176.

Sawyer,J.S.,1959:
The introduction of the effects of topography into methods of numerical forecasting.
Quart.J.Roy. Met.Soc. 85,31-43.

Smagorinsky,J., S.Manabe, and J.H.Holloway,Jr.,1965:
Numerical results from a nine-level general circulation model of the atmosphere.
Monthly Weather Review 93,727-768.

Wippermann,F.,1970:
The two constants in the resistance law for a neutral barotropic boundary layer of the atmosphere.
Beitr.Phys.Atm. 43,133-140.

B. REFERENCES ON FRONTOGENETIC PROCESSES

Bergeron,T.,1928:
Über die dreidimensional verknüpfende Wetteranalyse I.
Geofys. Publikasjoner, 6,Nr.6,1-111.

Graner,J.,1975:
Über die Bildung von Fronten, insbesondere in einem numerischen Modell.
Diplomarbeit, Meteorologisches Institut der Universität Hamburg, 83 pages.

Hoskins,B.J.,1972:
Atmospheric frontogenesis models; some solutions.
Quart. J.Roy.Met.Soc. 97,139-153.

Hoskins,B.J., F.P.Bretherton, 1972:
Atmospheric frontogenesis models; mathematic formulation and solution.
J.Atm.Sci. 29, 11-37.

Mudrick,S.,1974:
A numerical study of frontogenesis.
J.Atm.Sci. 31, 869-892.

Palmen,E., C.W.Newton,1969:
Atmospheric circulation systems.
Academic Press, New York-London.

Petterssen,S.,1936:
Contribution to the theory of frontogenesis.
Geofys.Publ. XI,6,5-27.

Saltzman,B., and Chung-Muh Tang,1974:
Mid-tropospheric frontogenesis in an amplifying baroclinic wave.
J.Atm.Sci. 31, 835-839.

Stone,P.H.,1966:
Frontogenesis by horizontal wind deformation fields.
J.Atm.Sci., 23,455-465.

Stone,P.H.,1969:
The meridional structure of baroclinic waves.
J.Atm.Sci.,26,376-389.

Williams,R.T.,1967:
Atmospheric frontogenesis: A numerical Experiment.
J.Atm.Sci. 24,627-641.

Williams,R.T., J.Plotkin,1968:
Quasi-geostrophic frontogenesis.
J.Atm.Sci. 25,201-206.

Williams,R.T.,1972:
Quasi-geostrophic versus non-geostrophic frontogenesis.
J.Atm.Sci. 29,3-10.

Williams,R.T.,1974:
Numerical simulation of steady-state fronts.
J.Atm.Sci. 31,1287-1295.

Benwell,G.R.R. and F.H. Bushby,1970:
A case study of frontal behaviour using a 10-level primitive equation model.
Quart. J.Roy.Met.soc. 96,287-296.